G-register exchange dynamics in guanine quadruplexes

Supplementary Information

Robert W. Harkness V, Anthony K. Mittermaier*

robert.harkness@mail.mcgill.ca

anthony.mittermaier@mcgill.ca*

Phone: (514) 398-3085

Fax: (514) 398-3797

McGill University, Department of Chemistry

801 Sherbrooke St. W., Montreal QC, H3A 0B8

Supplementary Methods

UV-Visible spectroscopy global fitting

The total absorbance *A(T)* for each trapped mutant was calculated as

$$A^{calc}(T) = P^{mut}(T) \times A_F(T) + \left(1 - P^{mut}(T)\right) \times A_U(T), \quad (1)$$

where A_F and A_U are the folded and unfolded absorbance baselines, respectively, and the relative population of the folded GQ, $P^{mut}(T)$, was determined as described in the Methods section (Equations 2-5). The absorbance baselines were assumed to depend linearly on temperature giving

$$A_F(T) = m_F T + b_F \quad (2)$$

and

$$A_U(T) = m_U T + b_U . \quad (3)$$

For the wild-type GQs undergoing GR exchange, the total absorbance, *A(T)* was calculated as

$$A^{calc}(T) = \left(\sum_i P_i^{WT}(T)\right) \times A_F(T) + \left(1 - \left(\sum_i P_i^{WT}(T)\right)\right) \times A_U(T), \quad (4)$$

where P_i^{WT} is the fraction of molecules populating the *i*th folded GR isomer. In the global fits, the UV-Vis data for all trapped mutants and the wild-type GQ were analyzed simultaneously. The absorbance profile for each trapped mutant was calculated according to Equations 2-5 in the Methods and Equations 1-3 in the Supplementary Methods with ΔH^{mut} and ΔS^{mut} defined independently for each mutant. The absorbance profile for the wild-type was calculated according to Equations 9 and 10 in the Methods and Equation 4 in the Supplementary Methods, using the thermodynamic parameters from the corresponding trapped mutants according to Equations 12 and 13 in the Methods. The folded baselines for all trapped mutants and the wild-type were optimized independently. The unfolded baseline intercept (b_U) was also optimized independently for each trapped mutant and wild-type, while the unfolded slope (m_U) was constrained to be identical for all absorbance profiles in the global fit. For a GQ with *N* GR isomers, the dataset comprised *N*+1 absorbance profiles (*N* mutants and the wild-type) and the global fit contained *N* values of ΔH and ΔS, *N*+1 values of m_F, b_F, and b_U, and a single value of m_U for a total of 5*N*+4 adjustable parameters. The parameters were varied to minimize the RSS

$$RSS = \sum_{j=1}^{N} \sum_{k} \left(A_j^{\exp}(T_k) - A_j^{calc}(T_k, \xi_j, \lambda_j) \right)^2 + \sum_{k} \left(A_{WT}^{\exp}(T_k) - A_{WT}^{calc}(T_k, \xi_{1..N}, \lambda_{WT}) \right)^2 \quad (5)$$

where T_k is the *k*th experimental temperature, $A_j^{exp}(T)$ and $A_j^{calc}(T)$ are the experimental and calculated absorbance profiles of the *j*th trapped mutant, $A_{WT}^{exp}(T)$ and $A_{WT}^{calc}(T)$ are the experimental and calculated absorbance profiles of the wild-type, $\xi_j=[\Delta H_j^{mut}, \Delta S_j^{mut}]$ are the folding parameters of the *j*th trapped mutant, and $\lambda_j=[b_{F,j}, m_{F,j}, b_{U,j}, m_U]$ and $\lambda_{WT}=[b_{F,WT}, m_{F,WT}, b_{U,WT}, m_U]$ are the coefficients of the linear folded and unfolded baselines of the trapped mutants and wild-type.

Assessing thermodynamic perturbations in trapping GR isomers

Monte Carlo computer simulations(1) of mutation-induced thermodynamic perturbations were performed as follows. A complete set of N ΔH^{WT} and ΔS^{WT} enthalpy and entropy values were selected as the "unperturbed" folding parameters of the N wild-type GR isomers, according to the optimized values extracted from the global fits. Simulated wild-type thermal denaturation data were then generated according to

$$A^{WT}\left(T_j\right) = f\left(\Delta H^{WT}_{1..N}, \Delta S^{WT}_{1..N}, T_j\right) + \sigma \times \varepsilon_j \tag{6}$$

where T_j is the *jth* temperature point, ε_j are random numbers with a mean of zero and standard deviation of 1, and f(x) represents Equations 9, 10, and 11 in the Methods (DSC) or 9 and 10 in the Methods and 4 in the Supplementary Methods (UV-Vis). σ is the experimental error in each point, estimated from the average reduced RSS of the individual fits, i.e.

$$\sigma = \sqrt{\left\langle \frac{RSS^{ind}}{DF} \right\rangle} \tag{7}$$

where DF is the degrees of freedom of each individual trapped mutant fit and angle brackets indicate the average. Perturbed trapped mutant denaturation data were then generated according to

$$A_i^{pert}\left(T_j\right) = f\left(\left(\Delta H_i^{WT} + \Delta\Delta E \times \varepsilon_{i,H}\right), \left(\Delta S_i^{WT} + \frac{\Delta\Delta E}{T_{ref}}\varepsilon_{i,S}\right), T_j\right) + \sigma \times \varepsilon_{i,j} \tag{8}$$

where $A_i^{pert}(T_j)$ is the data point at the jth temperature for the ith trapped mutant, ΔH_i^{WT} and ΔS_i^{WT} are the folding parameters for the corresponding wild-type GR isomer, $\Delta\Delta E$ governs the size of thermodynamic perturbations with units of kJ mol^{-1}, T_{ref}=298 K is a reference temperature, $\varepsilon_{i,H}$, $\varepsilon_{i,S}$, and $\varepsilon_{i,j}$ are random numbers with means of zero and standard deviations of 1, and f(x) represents Equations 4, 5, and 6 in the Methods (DSC) or 4 and 5 in the Methods and 1 in the Supplementary Methods (UV-Vis). The simulated data for the wild-type and complete set of trapped mutants were then globally fitted, iterating 10^3 times for each value of $\Delta\Delta E$ in the case of c-myc-Pu18 and 25 times in the case of PIM1. $\Delta\Delta E$ was varied from 0 to 5 kJ mol^{-1}, taking the average RSS from all iterations as the corresponding residual sum of squared differences. In order to evaluate the precision of the extracted parameters, identical Monte Carlo calculations were performed with $\Delta\Delta E=0$. The precision of the measurement was taken to be the reciprocal of the standard deviation of values obtained in all iterations.

Calculation of GR isomer numbers for GQ sequences from the Eukaryotic Promoter Database

We computed the number of possible GR isomers for each retrieved sequence as follows: The ith G-tract (i=1...4) comprising n_i consecutive dG residues can adopt R_i different registers with respect to a GQ core of three G-tetrads according to

$$R_i = n_i - 2 \ . \qquad (9)$$

For example, a G_3-tract has one possible register relative to the GQ core, a G_4-tract has two registers, with either the first or last dG occupying a loop position, and a G_5-tract has three registers. The total number of GR isomers for each retrieved GQ sequence was then computed as

$$R_T = \prod_{i=1}^{4} n_i \ . \tag{10}$$

For example the putative GQ-forming sequence 5'-$G_4N_mG_3N_mG_4N_mG_5$-3' has twelve possible GR isomers, $R_T = 2\times1\times2\times3 = 12$. Due to the maximum G-tract length of 5, the only numbers of GR isomers allowed in this analysis follow the rule $R_T=2^a\times3^b$, where a and b are integers, $0\leq(a,b)\leq4$ and $(a+b)\leq4$.

Predicting thermal upshifts

Assuming that the folding enthalpies of different GR isomers are approximately equal, the $T_m{}^{WT}$ of the wild-type ensemble is related to the T_m's of the individual GR isomers according to

$$T_m^{WT} = T_m \frac{\Delta S_{UF}}{(\Delta S_{UF} - \Delta\Delta S_{GR})} \tag{11}$$

where ΔS_{UF} is the unfolding entropy of a single GR isomer and the entropic contribution of exchanging among N GR isomers is given by $\Delta\Delta S_{GR}=R\ln(N)$.

Statistical analysis of errors

Errors in the group fitting parameters were calculated using the variance-covariance matrix(2) given by

$$\hat{V} = \frac{RSS}{DF}(\hat{X}\,\hat{W}\,\hat{X}^{T})^{-1} \tag{12}$$

where RSS is the residual sum of squared differences between experimental and fitted data points, DF is the degrees of freedom of the fit (N data points minus Φ parameters of the global fit) and $\hat{W}$ is a diagonal matrix of fitting weights, in this case all taken to be identically 1. $\hat{X}$ is a matrix of the first derivatives of the differences between the experimental and calculated data points (A^{exp} and A^{calc}), with respect to increments in each of the adjustable parameters (Φ_i). The element corresponding to the *i*th adjustable parameter and *j*th data point is thus

$$X_{ij} = \frac{\partial\left(A_j^{\exp} - A_j^{calc}\right)}{\partial\Phi_i} \equiv \frac{\partial\alpha_j}{\partial\Phi_i} \tag{13}$$

where A_j^{calc} is evaluated at the optimized set of parameters, Φ. The elements were evaluated numerically according to

$$X_{ij} \approx \frac{\partial\left(A_j^{\exp} - A_j^{calc}(+\Delta)\right) - \partial\left(A_j^{\exp} - A_j^{calc}(-\Delta)\right)}{2\Delta} \tag{14}$$

where $A_j^{calc}(\pm\Delta)$ is the *j*th data point calculated with all adjustable parameters set to their optimized values except, for the *i*th parameter, which is incremented by $\pm\Delta$. For a global fit with *N* data points and *M* adjustable parameters this gives

$$\hat{X} = \begin{bmatrix} \frac{\partial \alpha_1}{\partial \Phi_1} & \cdots & \frac{\partial \alpha_N}{\partial \Phi_1} \\ \vdots & \ddots & \vdots \\ \frac{\partial \alpha_1}{\partial \Phi_M} & \cdots & \frac{\partial \alpha_N}{\partial \Phi_M} \end{bmatrix} \tag{15}$$

The diagonal elements in $\hat{V}$ are the variances of the optimized fit parameters, while the off-diagonal elements are the covariances between the errors of the optimized parameters. The errors in group fitting populations were computed from the covariance matrix using a Monte Carlo approach(1). 10^4 sets of N thermodynamic parameters with random errors were generated according to:

$$\hat{V}' = \hat{L}\hat{L}^T \tag{16}$$

$$\begin{bmatrix} \Phi_1^{MC} \\ \vdots \\ \Phi_N^{MC} \end{bmatrix} = \begin{bmatrix} \Phi_1^{\exp} \\ \vdots \\ \Phi_N^{\exp} \end{bmatrix} + \hat{L} \begin{bmatrix} \varepsilon_1 \\ \vdots \\ \varepsilon_N \end{bmatrix} \tag{17}$$

where $\Phi^{exp}{}_{1...N}$ are the thermodynamic and baseline parameters extracted from a global fit, $\Phi^{MC}{}_{1...N}$ are the randomized Monte Carlo parameters for a single interation, $\hat{V}'$ is the portion of the covariance matrix corresponding to the variances and covariances in the thermodynamic parameters, $\varepsilon_{1...N}$ are random numbers with means of 0 and standard deviation 1, $\hat{L}$ is the lower triangular matrix from Cholesky decomposition satisfying Equation 16. The 10^4 sets of

thermodynamic parameters were used to generate 10^4 sets of populations. The standard deviations of the sets of populations were taken as their experimental errors.

Supplementary Text

Wild-type PIM1 thermal CD correction

In the case of PIM1, we found that the CD spectrum of the wild-type GQ contained a stronger signal at around 265 nm than did those of the mutants (Supplementary Figure 9a). This is unlikely to be due to intermolecular association of the DNA strands as it has previously been shown by gel electrophoresis that PIM1 forms a monomeric GQ at concentrations as high as 30 μM(3) while the CD analysis was performed at 10 μM. We collected CD spectra at 95 °C, a temperature at which both mutant and wild-type GQs are completely unfolded. The CD spectrum for the wild-type sequence retained a strong maximum at 265 nm, while those of the mutants were essentially flat with values of approximately zero (Supplementary Figure 9b). CD spectra of poly-dG/poly-dC duplex DNA also contain strong maxima at 265 nm while those of poly-dGdC do not(4). Therefore it appears that DNA strands with ≥5 consecutive dG residues produce this spectral signature in duplex, single-stranded, and GQ forms. To a first approximation, we corrected for this effect by subtracting the spectrum obtained at 95 °C from that obtained at 25 °C for the wild-type PIM1 GQ (Figure 2c,d and Supplementary Figure 6d-f).

Monte Carlo simulations of thermodynamics perturbations in PIM1 trapped mutants

We found that the global fit of PIM1 data is less sensitive to perturbation (Figure 5c and Supplementary Figure 19) than that of c-myc. Applying the same Monte Carlo procedure, we

obtained a maximum of perturbation of 2.4 kJ mol^{-1}, which is about 1.3% of the total folding enthalpy and 3.3% of the $\Delta\Delta H_F$ between most and least stable mutants. This result is not surprising, given that the global fit of PIM1 data involves many more GR isomers, such that opposing thermodynamic perturbations in different trapped mutants can essentially compensate for each other.

Supplementary Figures

c-myc Pu18	WT	5′-AGGGTGGGGAGGGTGGGG-3′		
	55dT	5′-AGGGTTGGGAGGGTTGGG-3′	55dI	5′-AGGGTIGGGAGGGTIGGG-3′
	35dT	5′-AGGGTGGGTAGGGTTGGG-3′	35dI	5′-AGGGTGGGIAGGGTIGGG-3′
	53dT	5′-AGGGTTGGGAGGGTGGGT-3′	53dI	5′-AGGGTIGGGAGGGTGGGI-3′
	33dT	5′-AGGGTGGGTAGGGTGGGT-3′	33dI	5′-AGGGTGGGIAGGGTGGGI-3′
VEGFA			WT	5′-GGGAGGGTTGGGGTGGG-3′
			1dI	5′-GGGAGGGTTIGGGTGGG-3′
			2dI	5′-GGGAGGGTTGGGITGGG-3′
PIM1	WT	5′-GGGCGGGGCGGGGGCGGGG-3′		
	1dT	5′-GGGCTGGGCTTGGGCTGGG-3′	1dI	5′-GGGCIGGGCIIGGGCIGGG-3′
	2dT	5′-GGGCTGGGCTTGGGCGGGT-3′	2dI	5′-GGGCIGGGCIIGGGCGGGI-3′
	3dT	5′-GGGCTGGGCTGGGTCTGGG-3′	3dI	5′-GGGCIGGGCIGGGICIGGG-3′
	4dT	5′-GGGCTGGGCTGGGTCGGGT-3′	4dI	5′-GGGCIGGGCIGGGICGGGI-3′
	5dT	5′-GGGCTGGGCGGGTTCTGGG-3′	5dI	5′-GGGCIGGGCGGGIICIGGG-3′
	6dT	5′-GGGCTGGGCGGGTTCGGGT-3′	6dI	5′-GGGCIGGGCGGGIICGGGI-3′
	7dT	5′-GGGCGGGTCTTGGGCTGGG-3′	7dI	5′-GGGCGGGICIIGGGCIGGG-3′
	8dT	5′-GGGCGGGTCTTGGGCGGGT-3′	8dI	5′-GGGCGGGICIIGGGCGGGI-3′
	9dT	5′-GGGCGGGTCTGGGTCTGGG-3′	9dI	5′-GGGCGGGICIGGGICIGGG-3′
	10dT	5′-GGGCGGGTCTGGGTCGGGT-3′	10dI	5′-GGGCGGGICIGGGICGGGI-3′
	11dT	5′-GGGCGGGTCGGGTTCTGGG-3′	11dI	5′-GGGCGGGICGGGIICIGGG-3′
	12dT	5′-GGGCGGGTCGGGTTCGGGT-3′	12dI	5′-GGGCGGGICGGGIICGGGI-3′

Supplementary Figure 1. G-quadruplex sequences investigated in this work. Red letters indicate bases that were mutated from dG>dX where dX = dT or dI.

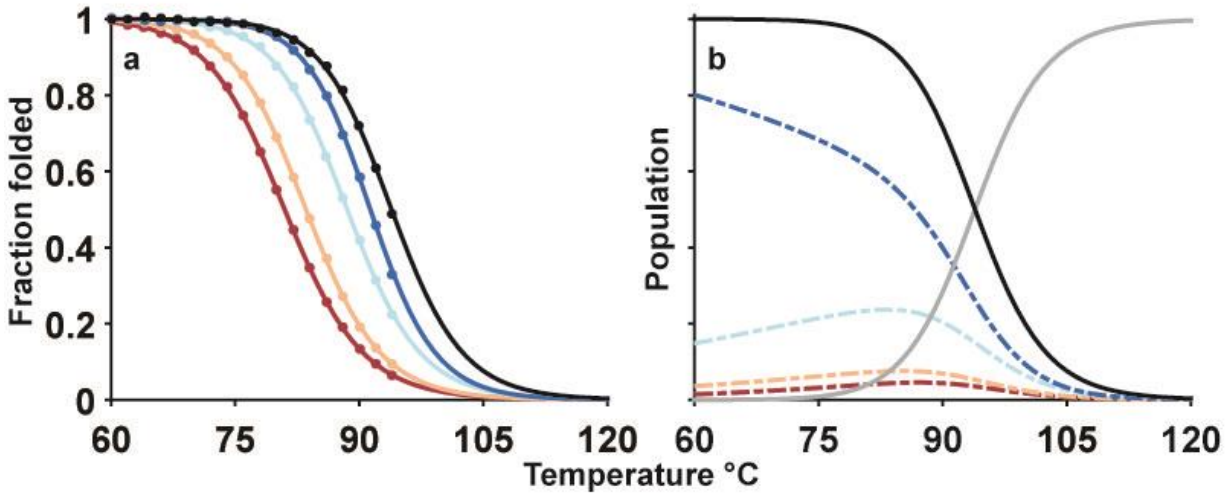

Supplementary Figure 2. UV-Vis thermal denaturation data for c-myc Pu18 wild-type and dT trapped mutant GQs. (a) Fraction of the folded state for the WT GQ and trapped mutants and (b) GR isomer populations extracted from a global fit of UV-Vis absorbance spectrophotometric data obtained with 130 mM K^+. The thermodynamic stabilities of the trapped mutants and the populations of the corresponding GR isomers rank in the same order as they do in the presence of lower K^+ concentrations. In (a), experimental data (points) and best fits (curves) are black (wild-type) and colored (trapped mutants). In (b), populations of the GR isomers are indicated by are colored dashed curves, the sum of folded isomer populations is indicated by the black curve, and population of the unfolded state is shown as a grey curve. Note that data could only be collected to 95 ºC. The extension of the curves in (a) and (b) to higher temperatures represents an experimentally inaccessible extrapolation.

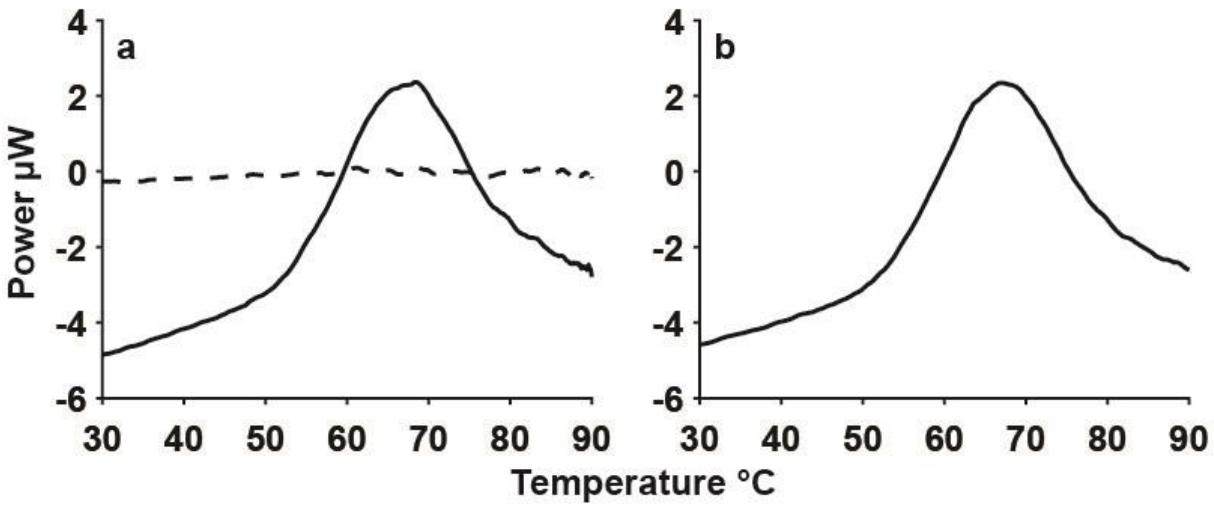

Supplementary Figure 3. DSC buffer baseline subtraction. In (a) the buffer baseline (black dashed line) is subtracted from the sample scan (c-myc Pu18 35 dG>dI trapped mutant, black line) to yield the buffer subtracted sample curve in (b).

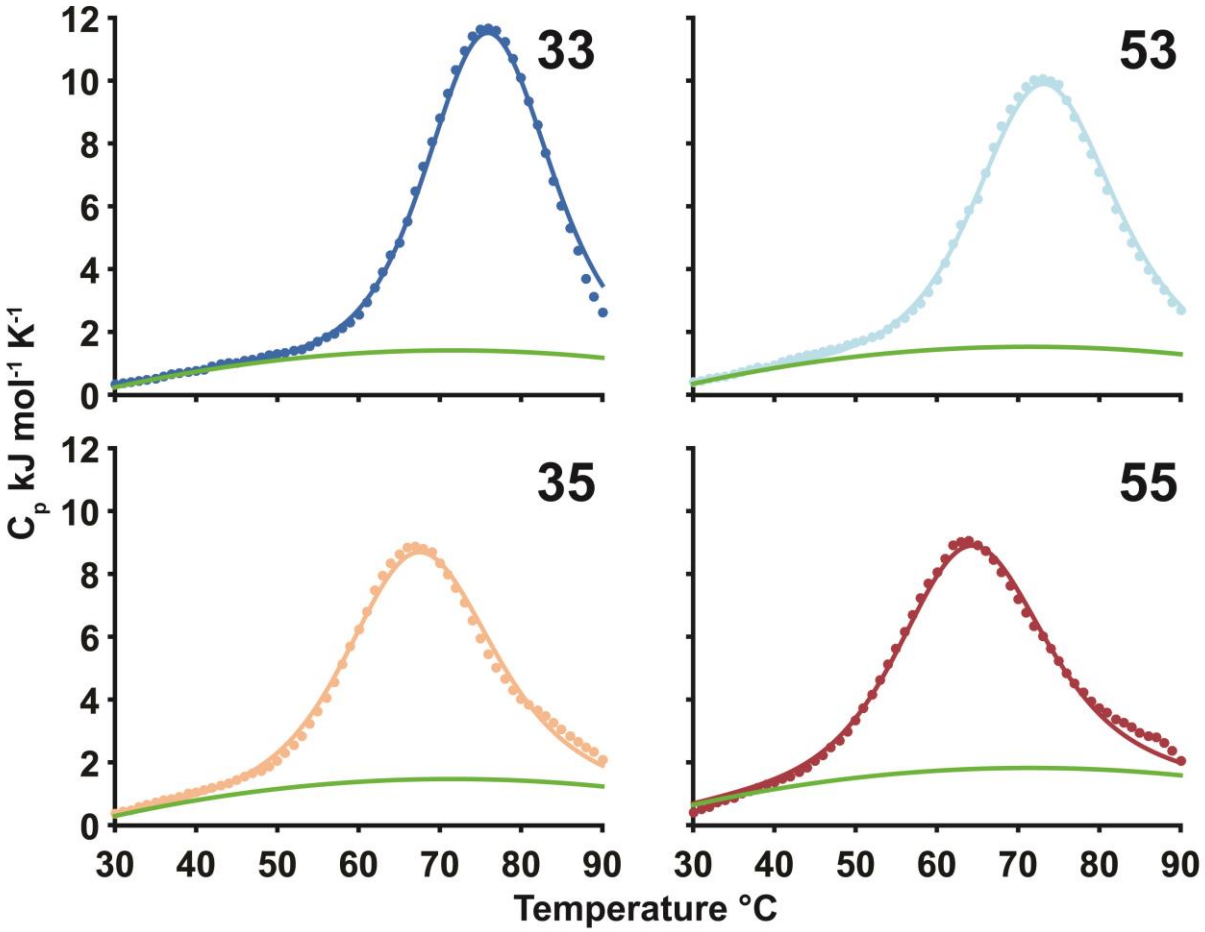

Supplementary Figure 4. Heat capacity curves from global analysis of DSC data. Experimental and fitted data are shown as filled colored circles and colored lines respectively. The second-order polynomial baseline is shown as green solid line. The four c-myc Pu18 dI trapped mutant thermograms are shown in order of decreasing stability.

Supplementary Table 1. Effect of ΔC_p on DSC global fit thermodynamics.

Sequence[a]	ΔC_p (J mol^{-1} K^{-1})	ΔH^a (kJ mol^{-1})	ΔS^a (J mol^{-1} K^{-1})
c-myc Pu18 55	240[b]	-165.0±0.1	-488.1±0.5
	1300[c]	-173.0±0.2	-510.4±0.5
	2100	-182.1±0.2	-536.7±0.6
c-myc Pu18 35	240[b]	-167.9±0.1	-492.3±0.4
	1300[c]	-176.7±0.2	-516.8±0.5
	2100	-186.7±0.2	-545.6±0.5
c-myc Pu18 53	240[b]	-183.5±0.2	-529.3±0.4
	1300[c]	-192.9±0.2	-555.4±0.5
	2100	-204.0±0.2	-586.9±0.5
c-myc Pu18 33	240[b]	-203.1±0.2	-581.4±0.4
	1300[c]	-211.9±0.2	-605.6±0.5
	2100	-222.5±0.2	-635.7±0.5

[a]Global fit results using dI trapped mutants. ΔH and ΔS at T_m of each trapped mutant.

[b]ΔC_p optimized in global fit.

[c]ΔC_p reported for human telomere GQ(5).

Errors were calculated according to the variance-covariance method (Supplementary Methods).

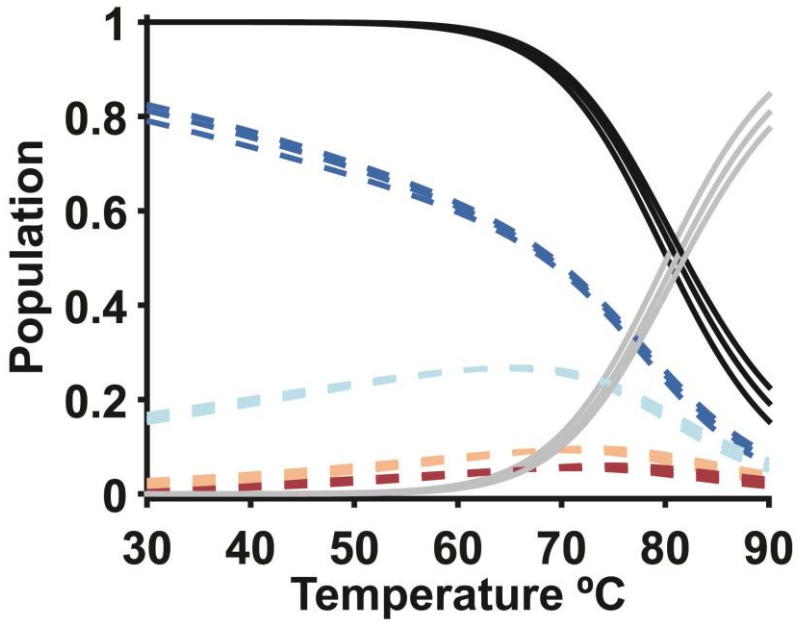

Supplementary Figure 5. Effect of ΔC_p on global fit populations. Global fits were performed with ΔC_p=0.24 (fit), 1.3 (telomere GQ), and 2.1 kJ mol^{-1} K^{-1} respectively. Populations of the GR isomers are indicated by colored dashed curves, the sum of folded isomer populations are indicated by the black curves, and populations of the unfolded state are shown as grey curves.

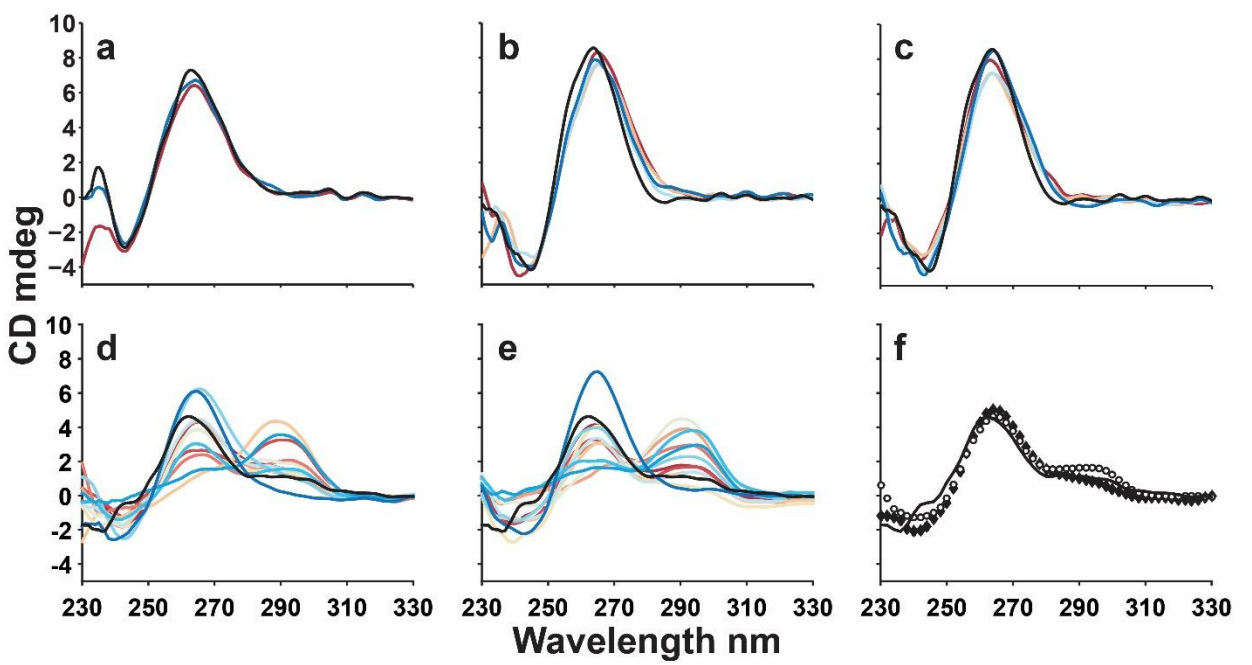

Supplementary Figure 6. Guanine quadruplex circular dichroism spectra. CD spectra for wild type (black) and trapped mutant (colored) VEGFA dG>dI (a), c-myc Pu18 dG>dT (b), c-myc Pu18 dG>dI (c), PIM1 dG>dT (d), and PIM1 dG>dI GQs (e). The color coding of trapped mutant data in (a-e) is the same as in Supplementary Figure 4. In (d-f), the solid line corresponds to the corrected wild-type PIM1 CD spectrum. In (f) population-weighted average spectra of dG>dT and dG>dI trapped mutants are shown with filled diamonds and empty circles, respectively.

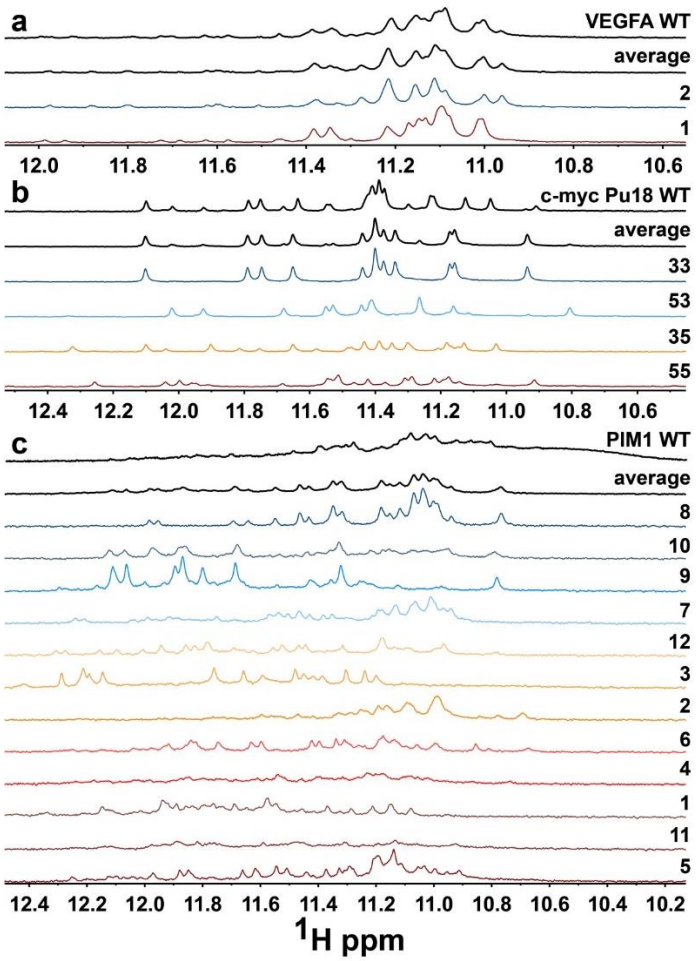

Supplementary Figure 7. 1D ^{1}H NMR spectra of WT and trapped mutant GQs. Imino proton regions of ^{1}H NMR spectra for VEGFA (a), c-myc Pu18 (b), and PIM1 (c) wild-type and dI trapped mutant GQs. Mutant spectra are ordered according to stability with more stable trapped mutants shown above less stable trapped mutants.

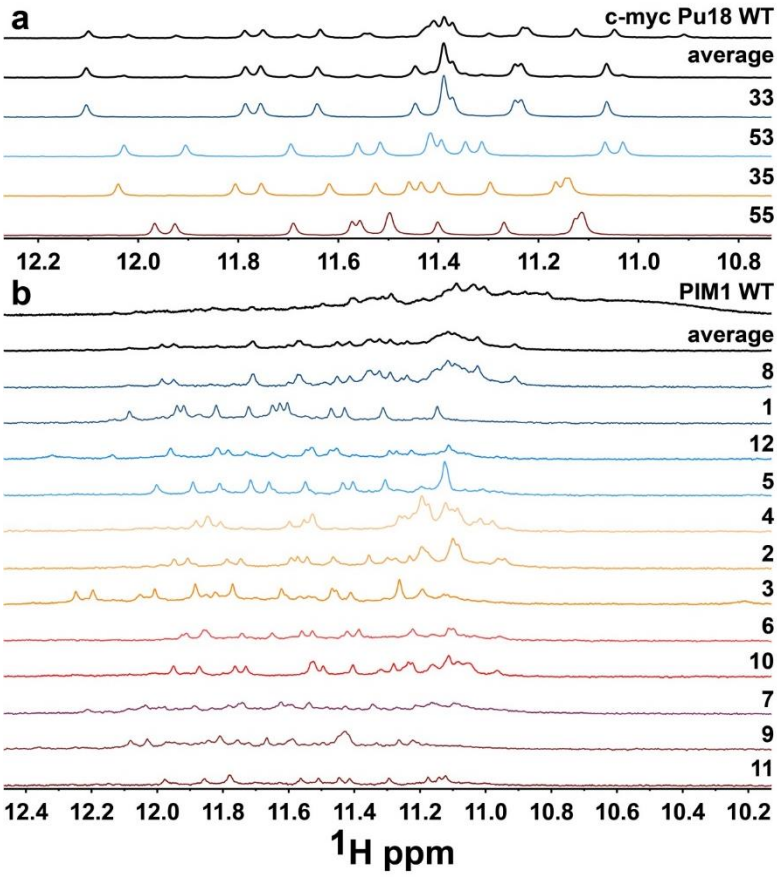

Supplementary Figure 8. ^{1}H NMR spectra for the WT and trapped dT mutant GQs. Imino proton regions of ^{1}H NMR spectra for c-myc Pu18 (a), and PIM1 (b) wild-type and dT trapped mutant GQs. Mutant spectra are ordered according to stability with more stable trapped mutants shown above less stable trapped mutants.

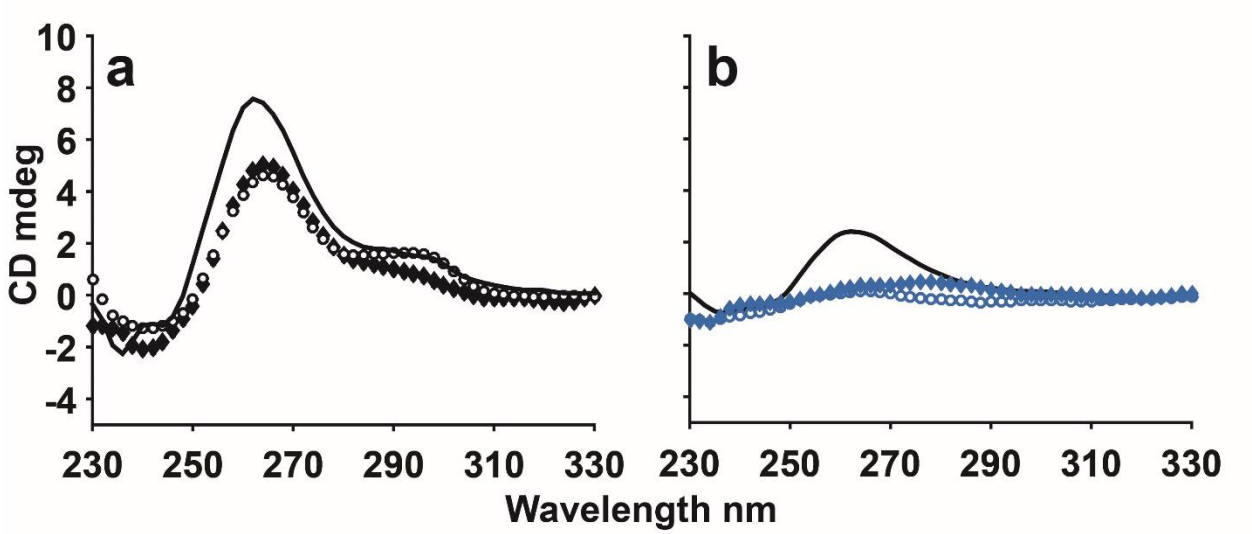

Supplementary Figure 9. Wild-type PIM1 CD correction. (a) CD spectrum of the wild-type PIM1 GQ (black curve) and the population-weighted average CD spectra of the dT (filled symbols) and dI (open symbols) trapped mutants at 25 °C. (b) CD spectra of the wild-type PIM1 GQ (black curve) and the most populated dT (filled symbols) and dI (open symbols) trapped mutants at 95 °C.

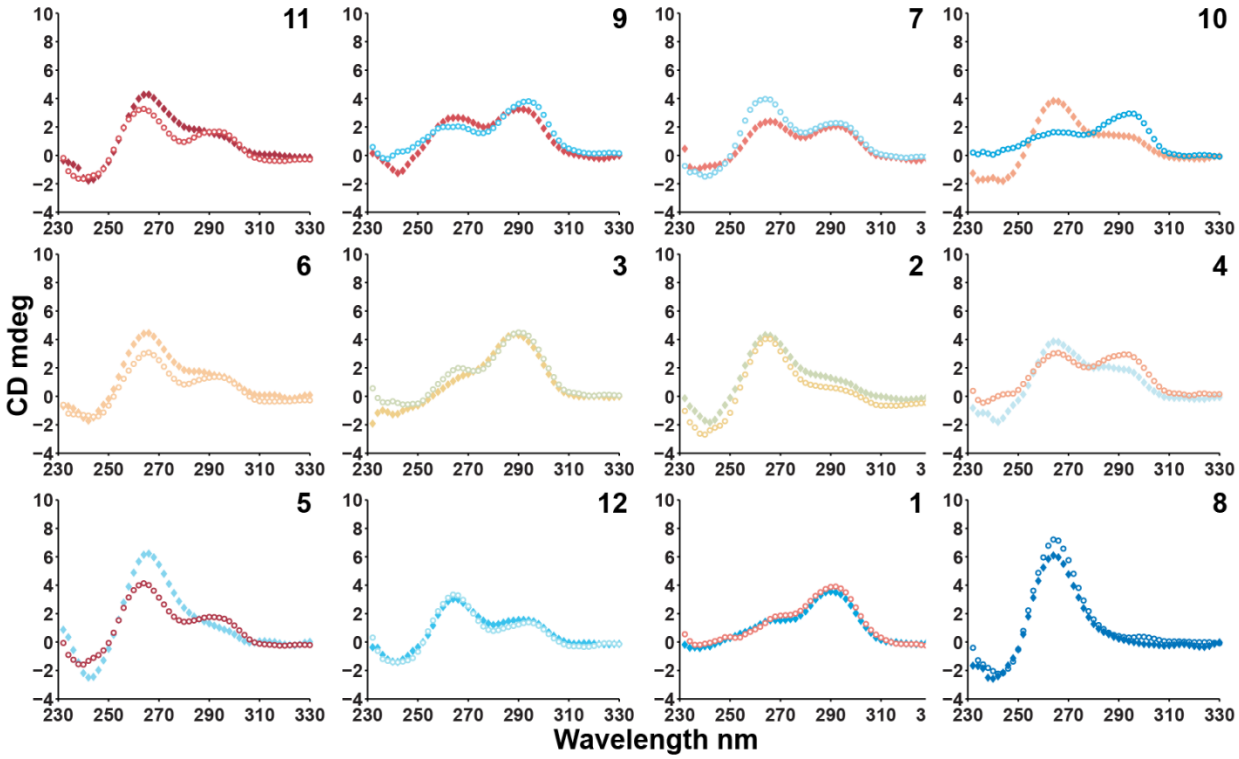

Supplementary Figure 10. PIM1 CD spectra. CD spectra of dG>dT (filled symbols) and dG>dI (open symbols) trapped mutants, indicated by the number in the upper right of each panel. The color coding matches that of Supplementary Figure 4.

Supplementary Table 2. Thermodynamic parameters obtained from two-state models and model-free analysis.

Sequence	c-myc Pu18 33 dG>dI	c-myc Pu18 53 dG>dI	c-myc Pu18 35 dG>dI	c-myc Pu18 55 dG>dI
$\Delta \boldsymbol{H}^{global,a}$ (kJ mol^{-1})	-202.5±0.1	-182.7±0.2	-167.1±0.2	-164.1±0.2
$\Delta \boldsymbol{H}^{cal,b}$ (kJ mol^{-1})	-207.2±3.2	-186.9±3.0	-162.6±2.8	-161.4±2.8
$\Delta \boldsymbol{H}^{VH,c}$ (kJ mol^{-1})	-207.8±0.3	-186.3±0.3	-169.7±0.4	-165.8±0.5
$\Delta \boldsymbol{S}^{global,d}$ (J mol^{-1} K^{-1})	-580.0±1.8	-527.3±1.8	-490.2±1.7	-486.1±1.7
$\Delta \boldsymbol{S}^{cal,e}$ (J mol^{-1} K^{-1})	-605.6±9.8	-551.3±9.1	-477.9±8.0	-476.8±8.2
$\Delta \boldsymbol{S}^{VH,f}$ (J mol^{-1} K^{-1})	-595.3±0.7	-538.1±0.9	-498.1±1.0	-490.7±1.5
$\Delta \boldsymbol{H}^{cal}/\Delta \boldsymbol{H}^{VH}$	1.00±0.02	1.00±0.02	0.96±0.02	0.97±0.02
$\Delta \boldsymbol{S}^{cal}/\Delta \boldsymbol{S}^{VH}$	1.02±0.02	1.03±0.02	0.96±0.02	0.97±0.02

[a]Enthalpy of folding extracted from the global analysis of DSC data.

[b]Calorimetric enthalpy calculated as area under the excess C_p curve. For the more stable 33 and 53 mutants, melting is incomplete at the maximum temperature used, thus ΔH^{cal} was calculated as twice the area under the lower-T half of the C_p curve, calculated from 25 °C to the T_m.

[c]van 't Hoff enthalpy calculated from the slope of the progress excess C_p curve(6).

[d]Entropy of folding extracted from the global analysis of DSC data.

[e]Calorimetric entropy calculated as area under the excess C_p/T curve. For the 33 and 53 mutants, ΔS^{cal} was calculated as twice the area under the lower-T half of the C_p/T curve, calculated from 25 °C to the T_m.

[f]van 't Hoff entropy calculated from the slope of the progress excess C_p/T curve(6).

Errors were calculated using the variance covariance method (global fit) or as the standard deviations of 10000 Monte Carlo iterations (calorimetric and van 't Hoff parameters).

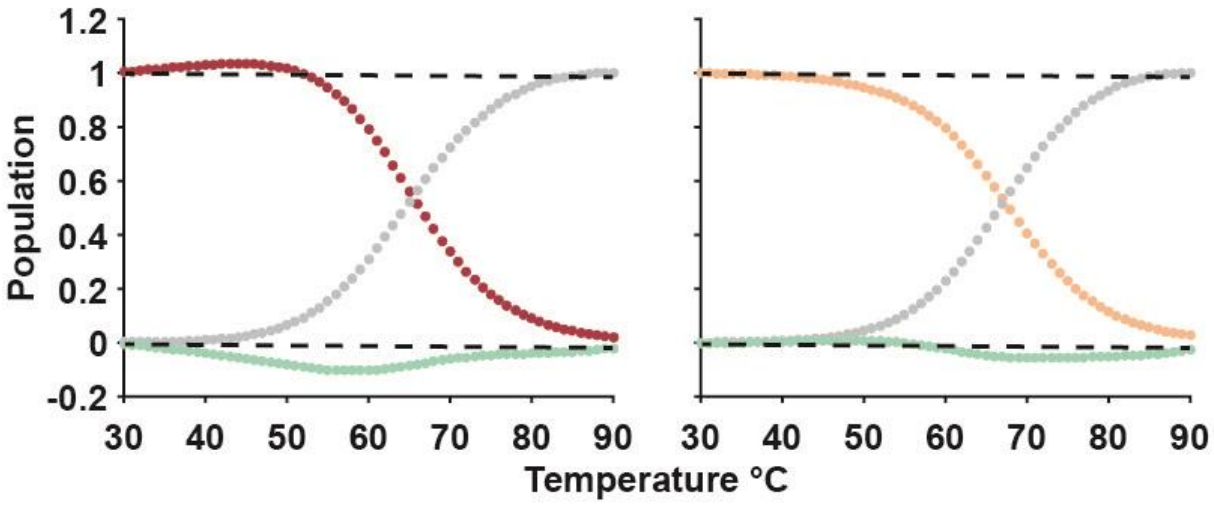

Supplementary Figure 11. Model-free deconvolution of experimental DSC data. The c-myc Pu18 55 and 35 dI trapped mutant DSC data (left and right panels respectively) were processed according to the Freire and Biltonen deconvolution method(7,8). Folded and unfolded populations (F and F_0) are shown as colored and grey filled circles respectively. 1-(F+F_0) is shown as turquoise filled circles. Dashed black lines indicate the 1 and 0 population limits.

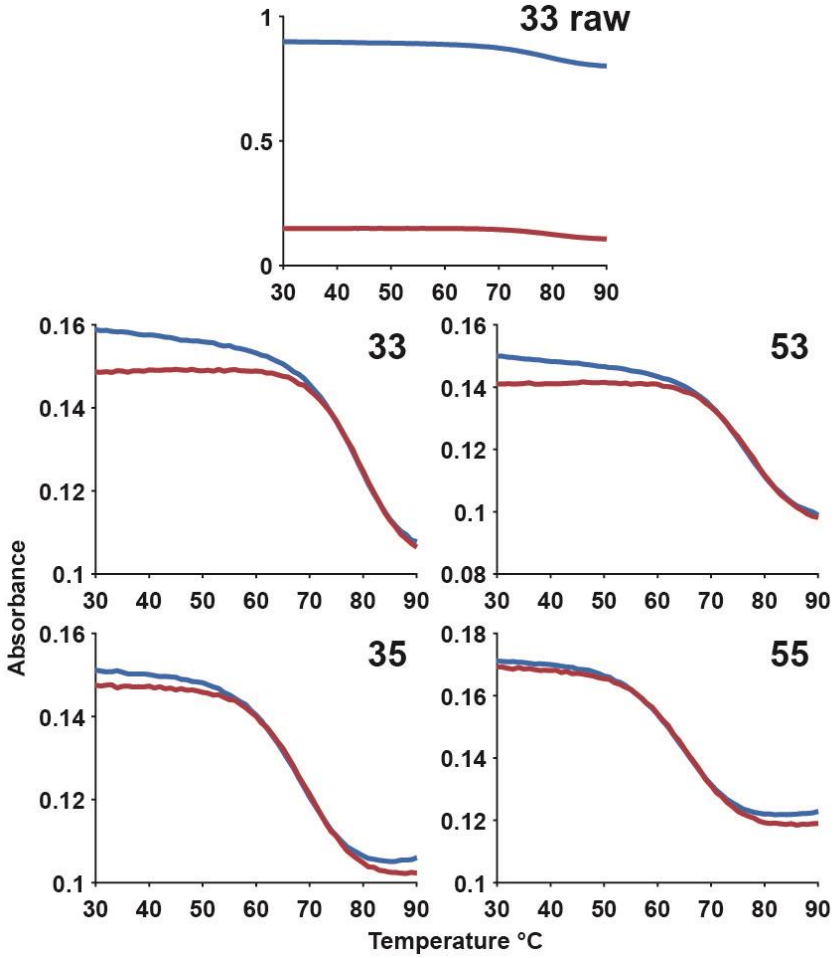

Supplementary Figure 12. Dual-wavelength absorbance melting for c-myc Pu18 trapped mutants. Raw absorbance data (top panel, 33 trapped mutant) at 260 nm have been vertically offset and scaled for comparison with the 295 nm data (lower four panels). Melting data at 260 and 295 nm are shown as blue and red curves respectively. Trapped dI mutant numbers are indicated in the top right corners. Experiments were performed using 5 μM strand concentrations.

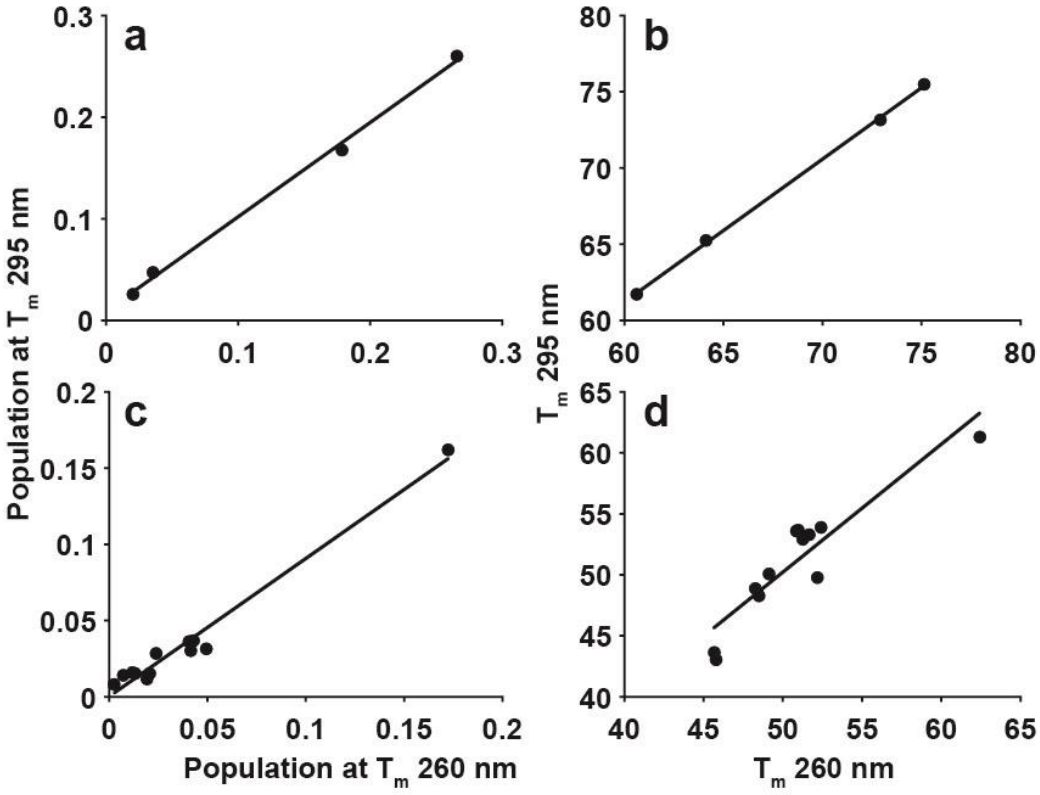

Supplementary Figure 13. Correlation of global fit parameters from 260 and 295 nm datasets. (a,b) The c-myc Pu18 trapped mutant populations at the T_m and T_ms at both wavelengths are strongly correlated (R=1.00 and 1.00 respectively). (c,d) The PIM1 trapped mutant populations at the T_m and T_ms at both wavelengths are strongly correlated (R=0.99 and 0.92 respectively). The dI trapped mutant data are shown here for both c-myc Pu18 and PIM1.

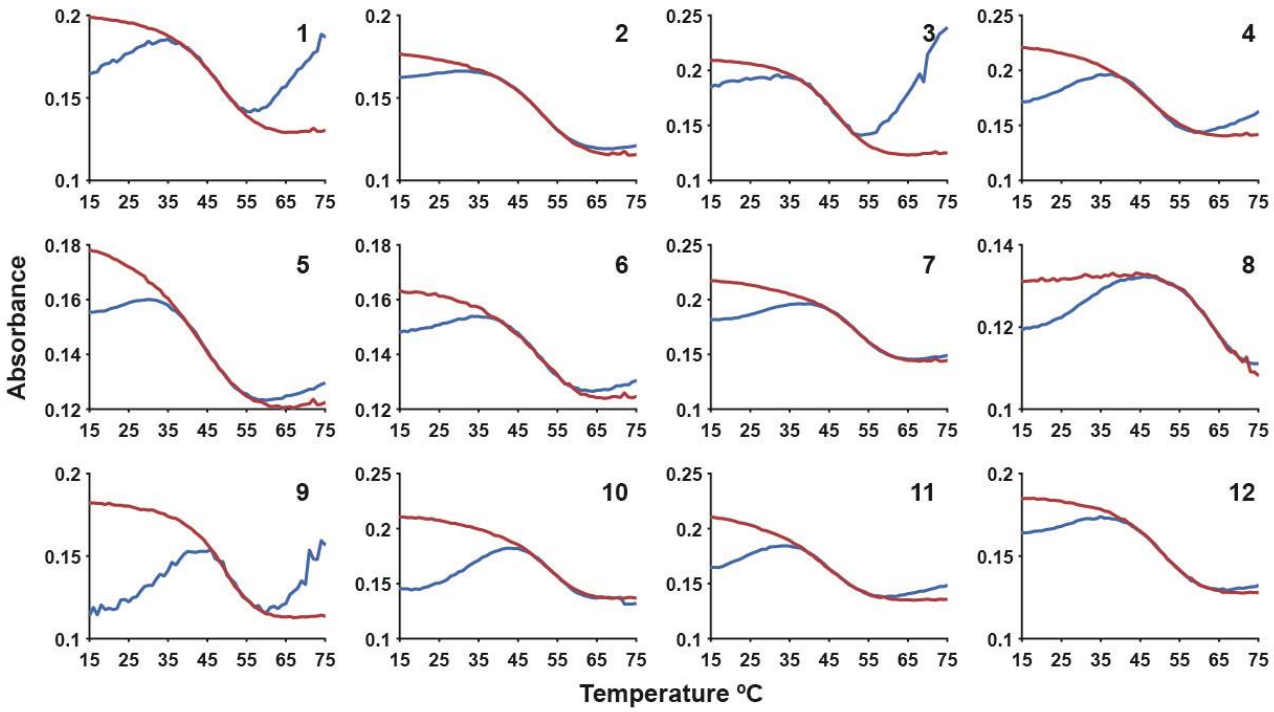

Supplementary Figure 14. Dual-wavelength absorbance melting for PIM1 trapped mutants. Absorbance data at 260 and 295 nm are shown as blue and red curves respectively. Raw absorbance data at 260 nm have been vertically scaled and offset, as above, for comparison with the 295 nm data. Trapped dI mutant numbers are indicated in the top right corners. Experiments were performed using 5 µM strand concentrations.

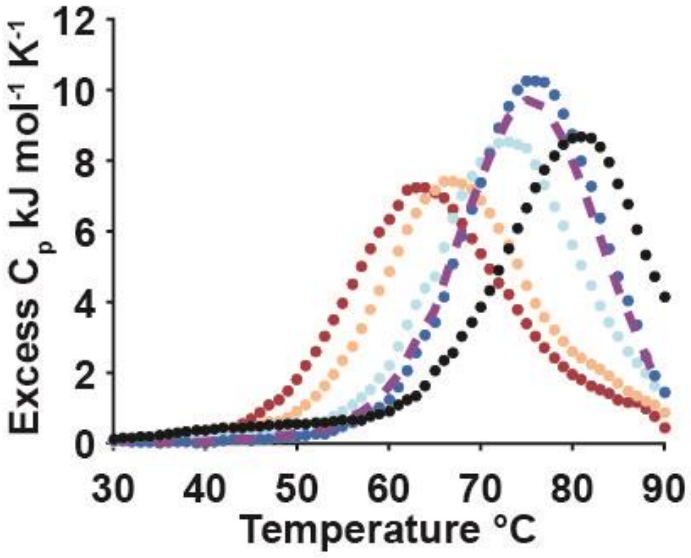

Supplementary Figure 15. Very slow timescale GR exchange would produce a thermal downshift. In the case of GR exchange that occurs slowly compared to the scan rate of the DSC, the thermogram of the WT GQ would be the population-weighted average of the individual thermograms of the GR isomers. To visualize this, the population-weighted average of the trapped mutant thermograms (c-myc Pu18 dG>dI) is shown by the purple dashed line (p_{33}=0.810, p_{53}=0.154, p_{35}=0.024, p_{55}=0.012 at 25 °C). The colored points correspond to the thermograms of the trapped mutants, and the black points correspond to the data for the WT GQ.

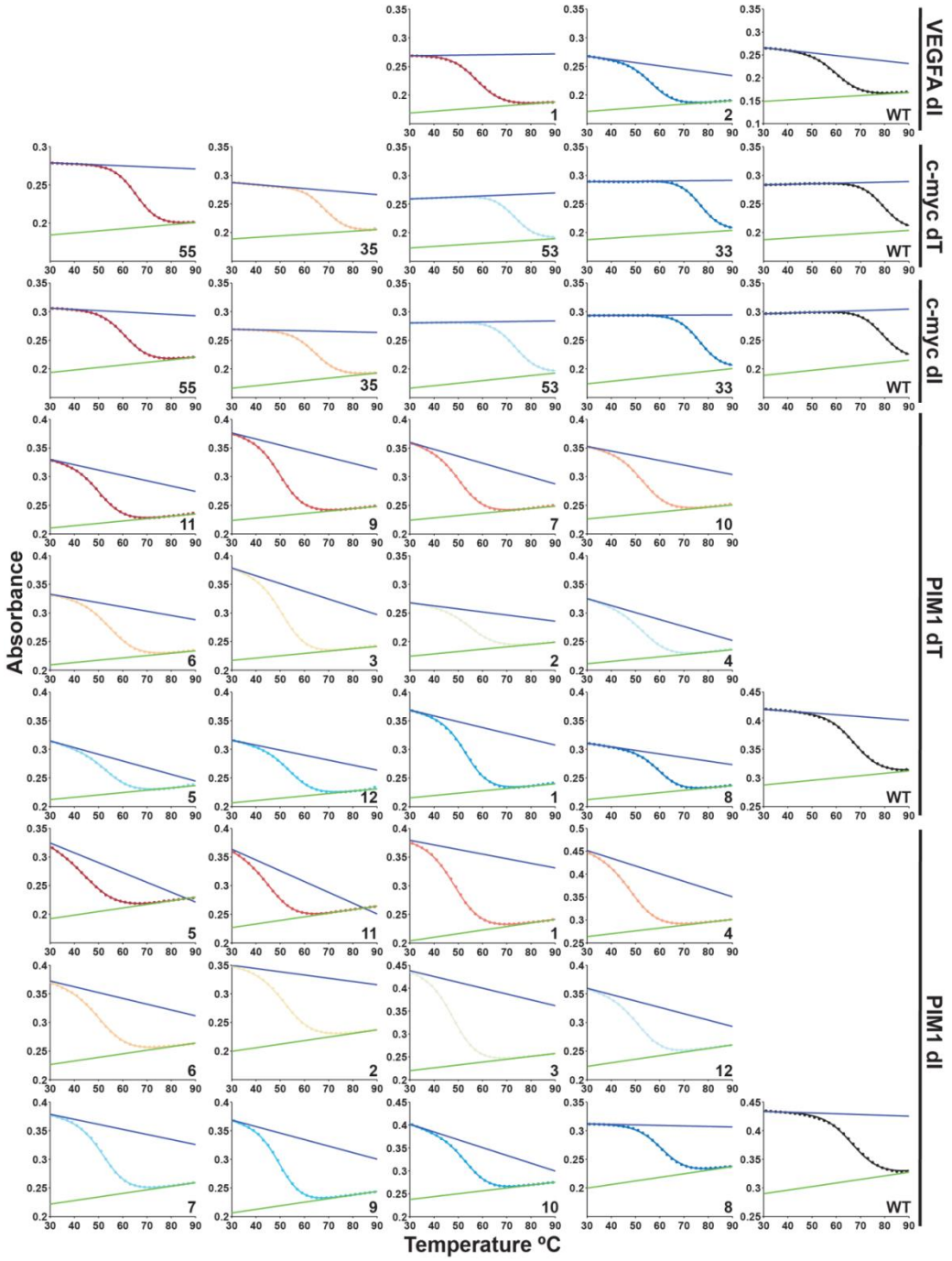

Supplementary Figure 16. Raw absorbance melting curves of the WT and trapped mutant c-myc Pu18, VEGFA, and PIM1 GQs. Color coding matches that of Figures 2 and 3. The fitted folded (blue line) and unfolded (green line) baselines for each melt are indicated.

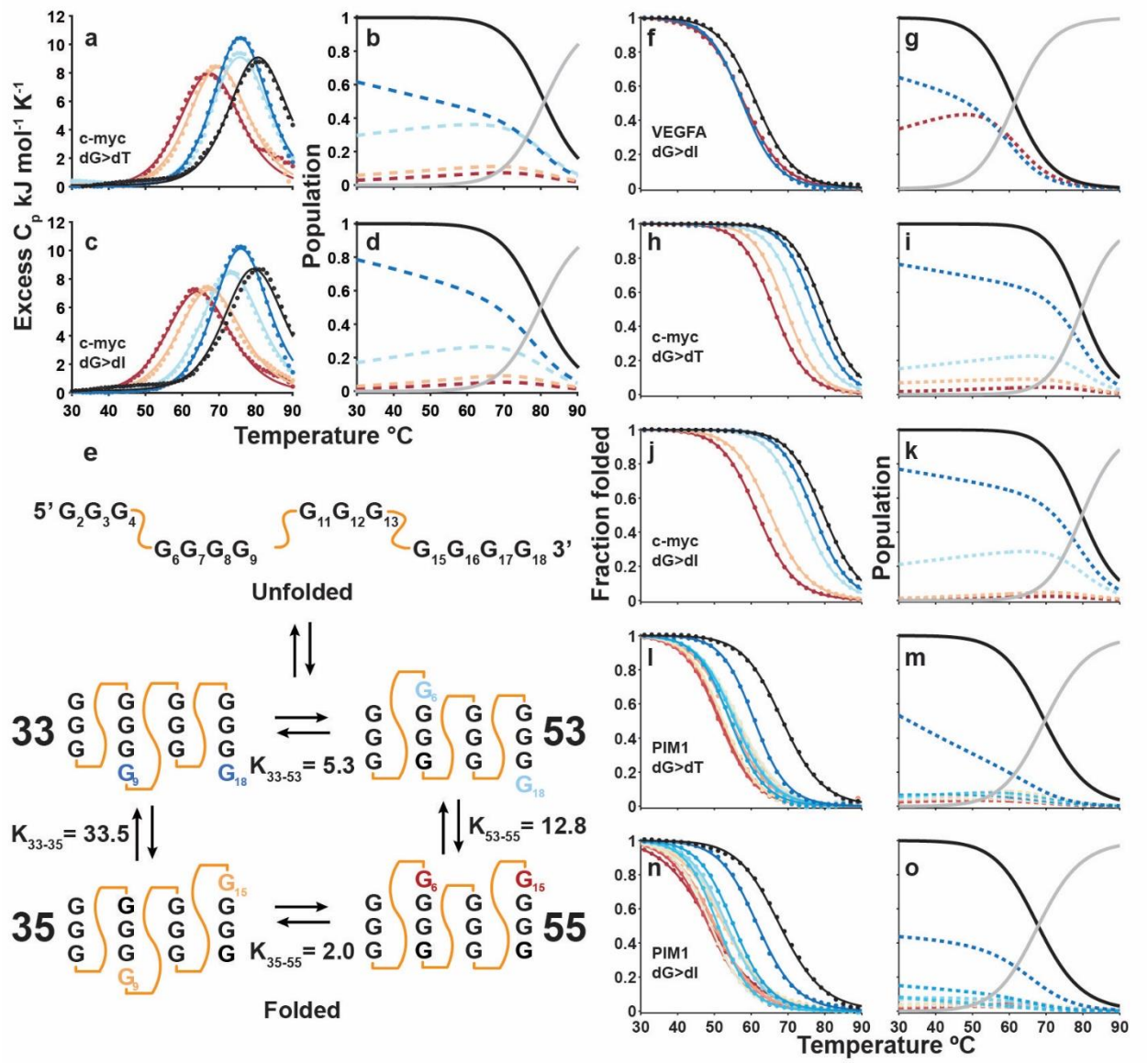

Supplementary Figure 17. Global fits of guanine quadruplex thermal denaturation data. Thermograms (points) and global best-fit lines (lines) obtained by DSC (a,c) and UV-Vis spectroscopy (f,h,j,l,n) for a complete set of dG>dT (a,h,l) and dG>dI (c,f,j,n) trapped mutant and wild-type GQs for c-myc Pu18 (a,c,h,j), VEGFA (f), and PIM1 (l,n). The GR isomer populations extracted from fits are plotted in the panels immediately to the right of the thermograms (b,d,g,i,k,m,o). The color scheme relates to the GR isomer population order extracted from the global fits, where dark blue to dark red indicates most to least populated GR isomer

respectively. Black corresponds to data for the wild-type GQ in (a,c,f,h,j,l,n) and the sum of all folded isomer populations in (b,d,g,i,k,m,o). In (b,d,g,i,k,m,o), grey curves correspond to the population of the unfolded state. (e) Cartoon of the c-myc Pu18 GQ undergoing exchange between 4 folded GR isomers and the unfolded state. $K_{X\text{-}Y}=P_X/P_Y$ is the equilibrium constant for isomers X and Y, shown as the values obtained from the trapped dI mutant fits. Errors are shown in Supplementary Table 5.

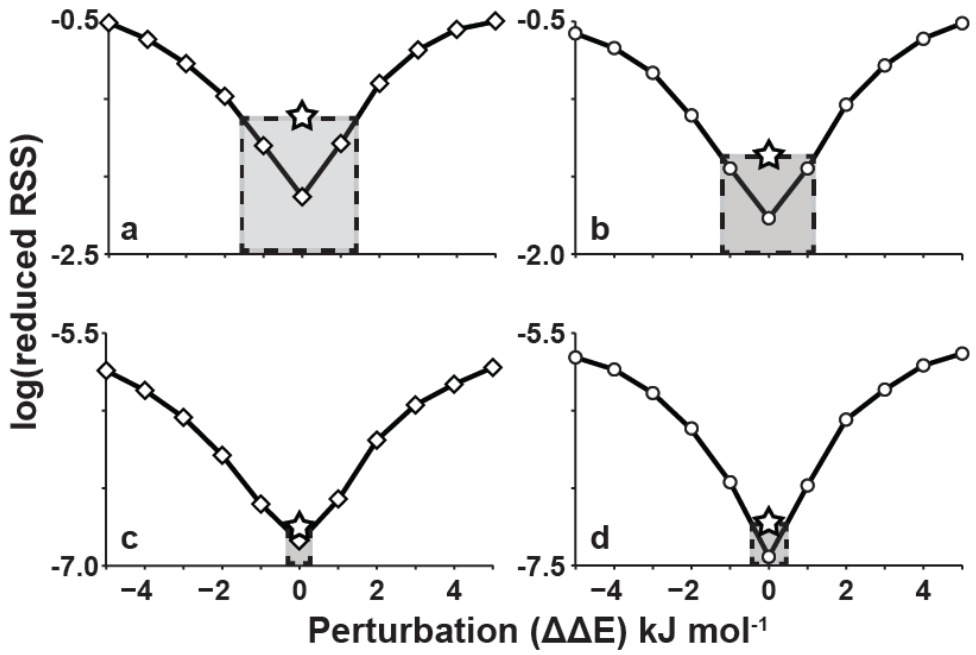

Supplementary Figure 18. Sensitivity of the c-myc Pu18 global fit to thermodynamic perturbations. Plot of average reduced RSS (RSS/DF) obtained for global fits of simulated c-myc Pu18 GQ (a,b) DSC and (c,d) UV-Vis data in which the folding ΔH and $T_0\Delta S$ of trapped mutants differ from those of the corresponding wild-type GR isomer by random perturbations with a mean of zero and standard deviation of $\Delta\Delta E$ kJ mol^{-1} (1000 iterations). The reduced RSS is the residual sum of squared difference between simulated data and the fits, divided by the number of degrees of freedom of the fit. The stars correspond to the experimental reduced RSS^{exp} values, while the set of ΔΔE giving <RSS> ≤ RSS^{exp} gives the ranges of thermodynamic perturbations consistent with our data. Simulations for the dG>dT and dG>dI trapped mutant datasets are in panels (a,c) and (b,d), respectively.

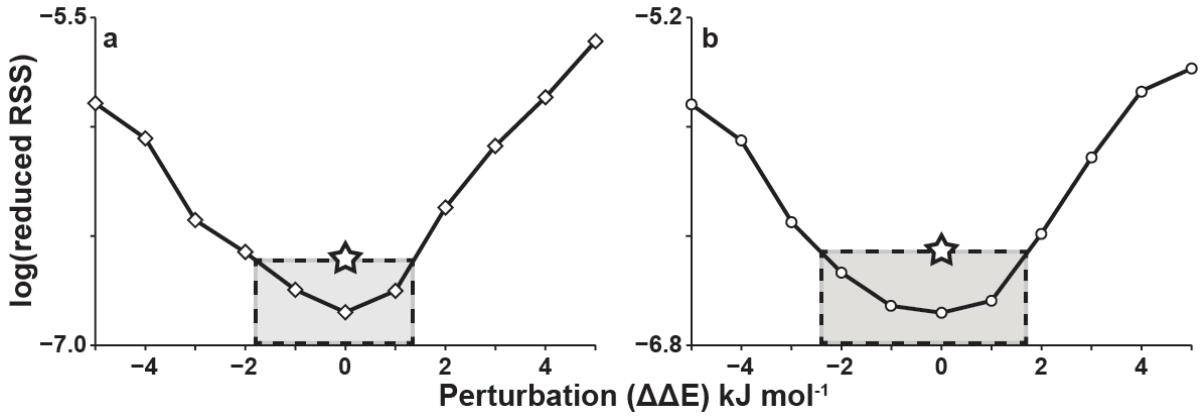

Supplementary Figure 19. Sensitivity of the PIM1 global fit to thermodynamic perturbations. Plot of average reduced RSS (RSS/DF) obtained for global fits of simulated PIM1 GQ UV-Vis data in which the folding ΔH and $T_0\Delta S$ of trapped mutants differ from those of the corresponding wild-type GR isomer by random perturbations with a mean of zero and standard deviation of $\Delta\Delta E$ kJ mol^{-1} (25 iterations). The stars correspond to the experimental reduced RSS^{exp} values, while the set of $\Delta\Delta E$ giving <RSS> ≤ RSS^{exp} gives the ranges of thermodynamic perturbations consistent with our data. Simulations for the dG>dT (a) or dG>dI (b) trapped mutant datasets are shown in (a) and (b), respectively.

Supplementary Table 3. **Thermodynamic parameters from the DSC global fitting of the c-myc Pu18 GQ.**

Sequence	**dT** ΔH kJ mol^{-1}	**dI** ΔH kJ mol^{-1}	**dT** ΔS J mol^{-1} K^{-1}	**dI** ΔS J mol^{-1} K^{-1}	**dT** T_m °C	**dI** T_m °C
c-myc Pu18 55	-175.3±0.2	-164.1±0.2	-514.3±0.6	-486.1±1.7	67.90±0.02	64.70±0.02
c-myc Pu18 35	-181.2±0.2	-167.1±0.2	-528.0±0.4	-490.2±1.7	70.20±0.02	67.90±0.02
c-myc Pu18 53	-191.9±0.2	-182.7±0.2	-550.0±0.4	-527.3±1.8	76.00±0.03	73.50±0.02
c-myc Pu18 33	-205.9±0.2	-202.5±0.1	-590.0±0.5	-580.0±1.8	76.00±0.01	76.20±0.02

Errors were calculated as stated in the Supplementary Methods section.

Supplementary Table 4. Thermodynamic parameters extracted from the global fit of UV-Vis data for the c-myc Pu18, VEGFA, and PIM1 GQs.

Sequence	**dT** ΔH kJ mol^{-1}	**dI** ΔH kJ mol^{-1}	**dT** ΔS J mol^{-1} K^{-1}	**dI** ΔS J mol^{-1} K^{-1}	**dT** T_m °C	**dI** T_m °C
c-myc Pu18 55	-210.4±2.3	-179.4±1.1	-619.9±6.4	-539.6±2.9	66.2±0.1	62.00±0.04
c-myc Pu18 35	-224.8±2.5	-183.2±1.2	-656.2±6.9	-543.1±3.2	69.4±0.1	65.60±0.04
c-myc Pu18 53	-221.1±2.3	-202.9±1.2	-638.0±6.4	-588.0±3.1	73.6±0.1	74.40±0.04
c-myc Pu18 33	-236.3±2.1	-215.6±1.3	-674.6±5.9	-616.0±3.5	77.3±0.1	77.20±0.03
VEGFA-1	-	-173.2±2.2	-	-520.7±5.8	-	58.1±0.1
VEGFA-2	-	-193.3±2.9	-	-584.8±7.8	-	57.7±0.1
PIM1-1	-178.6±2.4	-155.5±1.5	-547.8±7.2	-482.4±4.5	54.5±0.1	50.0±0.1
PIM1-2	-150.3±3.5	-149.2±1.7	-455.8±10.3	-457.2±4.9	56.7±0.2	53.4±0.2
PIM1-3	-171.9±2.3	-174.7±1.4	-530.1±6.9	-542.5±4.2	52.5±0.1	49.1±0.1
PIM1-4	-157.2±3.4	-153.3±1.5	-478.0±10.1	-475.3±4.4	55.7±0.2	50.2±0.2

PIM1-5	-159.3±4.0	-127.0±1.8	-492.5±11.9	-392.5±5.1	55.9±0.2	49.4±0.4
PIM1-6	-153.5±2.6	-144.7±1.9	-461.8±7.6	-444.6±5.6	56.4±0.2	52.9±0.2
PIM1-7	-164.7±2.7	-172.8±1.9	-510.5±8.1	-528.5±5.7	52.4±0.1	53.6±0.1
PIM1-8	-200.3±3.9	-176.2±2.3	-596.0±11.5	-526.8±6.7	61.2±0.1	61.8±0.1
PIM1-9	-166.7±2.3	-194.7±2.1	-513.7±6.8	-599.8±6.3	51.4±0.2	51.1±0.1
PIM1-10	-162.0±2.7	-183.1±2.2	-489.7±7.9	-558.2±6.5	54.7±0.2	55.3±0.1
PIM1-11	-159.0±3.0	-158.5±2.3	-488.4±8.9	-492.6±6.7	51.8±0.2	48.4±0.3
PIM1-12	-162.8±3.3	-166.6±2.3	-494.7±9.3	-511.2±6.7	55.8±0.5	53.3±0.2

Errors were calculated as stated in the Supplementary Methods section.

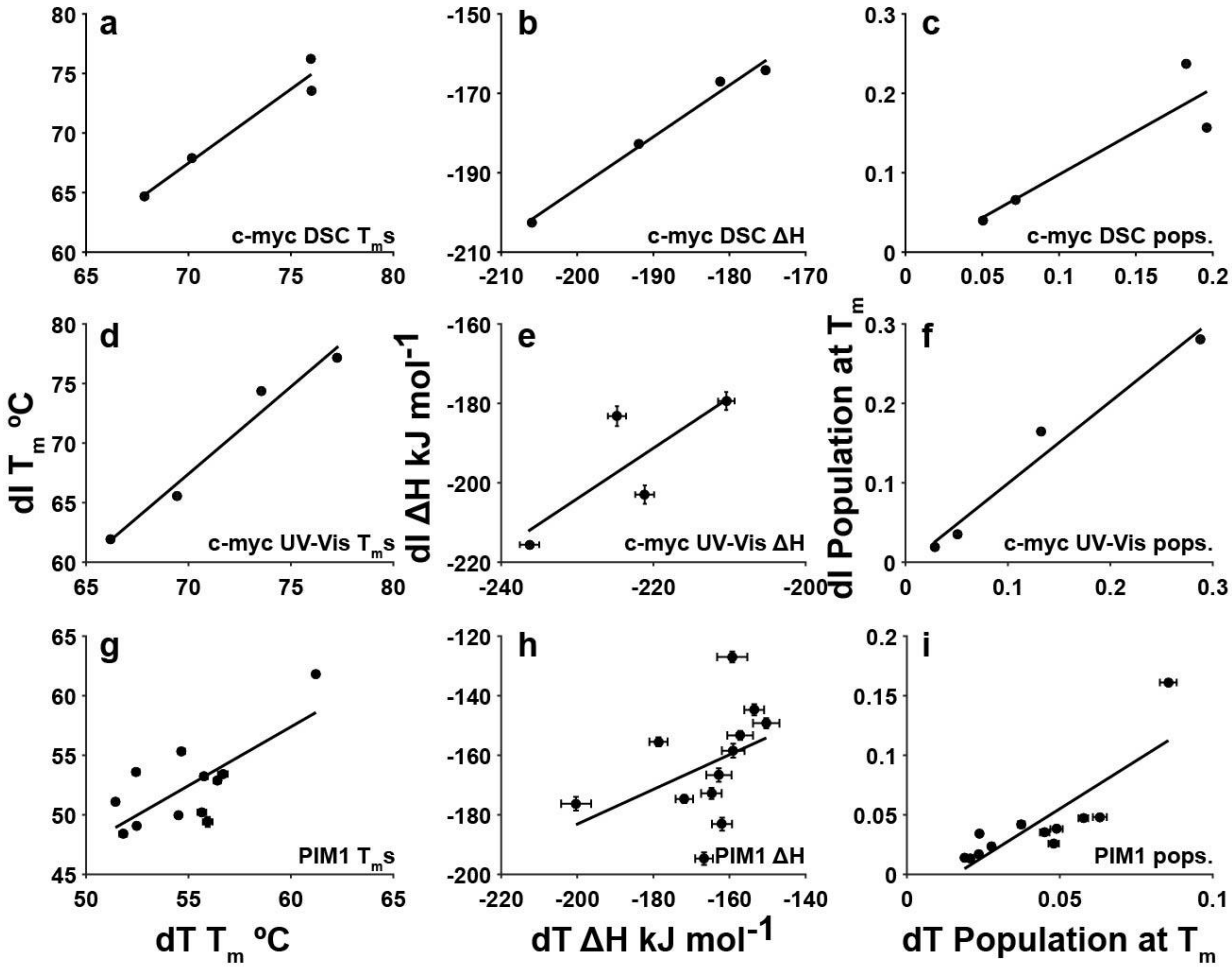

Supplementary Figure 20. Correlation of folding parameters extracted from global fits of dT and dI trapped mutants of the c-myc Pu18 and PIM1 GQs. Thermodynamic parameters from the global fits of c-myc Pu18 DSC data are strongly correlated (r=0.98, 0.99, 0.90 in panels a-c). Thermodynamic parameters from global fits of the c-myc Pu18 UV-Vis data are similarly well-correlated (r=0.99, 0.80, 0.99 in panels d-f). The parameters extracted from PIM1 UV-Vis data are reasonably well-correlated (r=0.73, 0.42, 0.83 in panels g-i). Errors are smaller than the symbols in some plots.

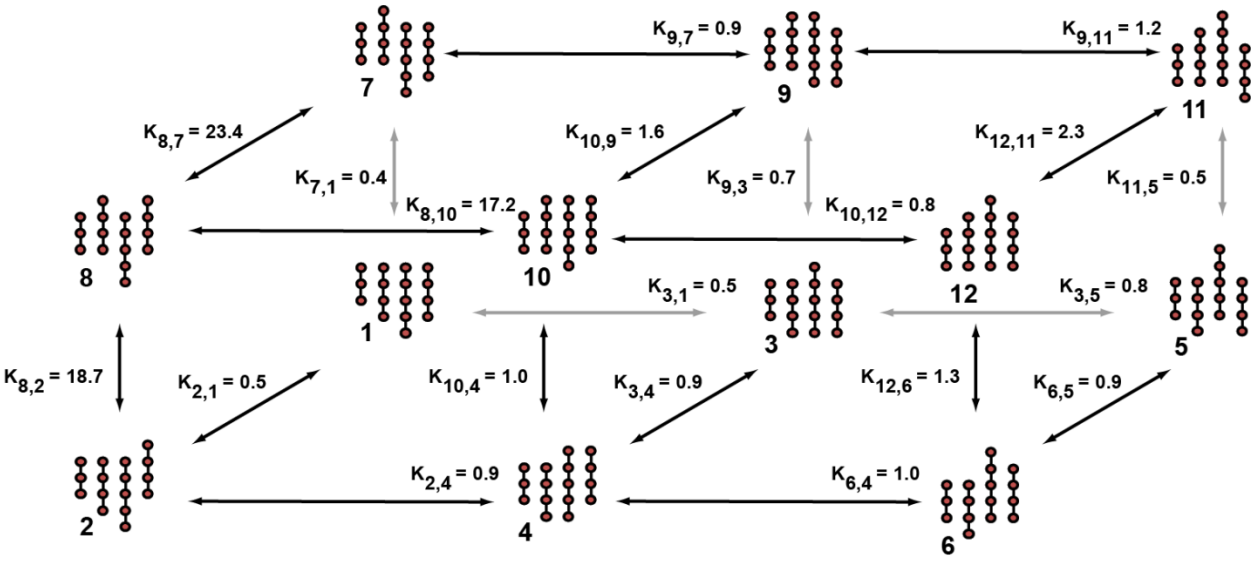

Supplementary Figure 21. Coupled GR exchange in the PIM1 GQ. dG residues are depicted as filled red circles and loop residues have been omitted for clarity. K_{ex} were calculated as the ratios of GR isomer populations. For example, $K_{X,Y}$ = [X]/[Y].

Supplementary Table 5. GR exchange equilibrium constants for the c-myc Pu18 dT and dI trapped mutants calculated from the DSC and UV-Vis global fitting parameters.

Equilibrium	DSC dT K_{ex}	DSC dI K_{ex}	UV-Vis dT K_{ex}	UV-Vis dI K_{ex}
33-53	2.3±0.0	5.3±0.1	5.6±1.1	3.8±0.4
53-55	11.2±0.2	12.8±0.3	9.0±1.5	38.5±3.3
35-55	2.1±0.0	2.0±0.0	4.3±0.7	2.4±0.2
33-35	12.4±0.2	33.5±0.4	11.7±2.3	60.6±5.2

The exchange equilibria follow the cycle given in the main text. K_{ex} were calculated at 25 °C from population ratios extracted from the DSC and UV-Vis global fitting, e.g. $K_{33\text{-}53}=P_{33}/P_{53}$. All K_{ex} have been expressed as >1 for ease of comparison. Errors are smaller than one decimal place for certain K_{ex}. Errors were calculated as stated in the Supplementary Methods section.

Supplementary Table 6. GR exchange equilibrium constants for the PIM1 dT and dI trapped mutants extracted from the extracted UV-Vis global fits.

Equilibrium	dT K_{ex}	dI K_{ex}
8,2	18.7±2.7	13.2±1.9
2,4	0.9±0.1	1.5±0.2
10,4	1.0±0.1	7.4±0.9
8,10	17.2±2.3	2.7±0.4
6,4	1.0±0.1	1.2±0.1
12,6	1.3±0.2	2.3±0.3
10,12	0.8±0.1	2.7±0.4
7,1	0.4±0.0	3.5±0.4
3,1	0.5±0.1	1.5±0.1
9,3	0.7±0.1	2.9±0.3
9,7	0.9±0.1	1.3±0.2
3,5	0.8±0.1	4.0±0.5
11,5	0.5±0.1	2.2±0.3
9,11	1.2±0.1	5.3±0.7
2,1	0.5±0.1	1.5±0.2
3,4	0.9±0.1	1.6±0.1
6,5	0.9±0.1	3.1±0.4
8,7	23.4±2.7	5.6±0.8
10,9	1.6±0.1	1.6±0.2
12,11	2.3±0.3	3.2±0.5

K_{ex} were calculated as the ratios of GR isomer populations at 25 °C. For example, $K_{X,Y}$ = [X]/[Y].

Errors were calculated as stated in the Supplementary Methods section.

References

1. Tellinghuisen, J. (2000) A Monte Carlo study of precision, bias, inconsistency, and non-Gaussian distributions in nonlinear least squares. *J Phys Chem A*, **104**, 2834-2844.
2. Tellinghuisen, J. (2001) Statistical error propagation. *J Phys Chem A*, **105**, 3917-3921.
3. Kumar, N. and Maiti, S. (2008) A thermodynamic overview of naturally occurring intramolecular DNA quadruplexes. *Nucleic Acids Res.*, **36**, 5610-5622.
4. Kypr, J., Kejnovska, I., Renciuk, D. and Vorlickova, M. (2009) Circular dichroism and conformational polymorphism of DNA. *Nucleic Acids Res.*, **37**, 1713-1725.
5. Boncina, M., Lah, J., Prislan, I. and Vesnaver, G. (2012) Energetic basis of human telomeric DNA folding into G-quadruplex structures. *J. Am. Chem. Soc.*, **134**, 9657-9663.
6. Saboury, A.A. and Moosavi-Movahedi, A.A. (1994) Clarification of calorimetric and van't hoff enthalpies for evaluation of protein transition states. *Biochemical Education*, **22**, 210-211.
7. Freire, E., Biltonen, R. L. (1978) Statistical mechanical deconvolution of thermal transitions in macromolecules. I. Theory and application to homogeneous systems. *Biopolymers*, **17**, 463-479.
8. Spink, C.H. (2015) The deconvolution of differential scanning calorimetry unfolding transitions. *Methods*, **76**, 78-86.